Volume 1 | Number 1 | Jan 2013 | Pages 1–100

Nanoscale

www.rsc.org/nanoscale

ROYAL SOCIETY OF CHEMISTRY

ROYAL SOCIETY OF CHEMISTRY

www.rsc.org/nanoscale

Journal Name

Direct Coating of Mesoporous Titania on CTAB-capped Gold Nanorods

Junwei Zhao,[a,b] Pengyu Xu,[a] Yue Li,[a] Jian Wu,[a] Junfei Xue,[a] Qiannan Zhu,[a] Xuxing Lu,[a] Weihai Ni[a]*

We demonstrate a CTAB-templated approach towards direct coating of mesoporous titania on gold nanorods in aqueous solutions. The formation of the mesoporous shell is found to be closely correlated with CTAB concentration and amount of the tinania precursor. This approach can be readily extended to form mesoporous titania shells on other CTAB-capped nanoparticles.

Titania (TiO_2) is a widely used semiconductor photocatalyst for a variety of solar-driven energy and environment applications. Unfortunately, the wide band gap of TiO_2, 3.2 eV, places a limit on the conversion efficiency of the solar energy because only ultraviolet (UV) part of sunlight can be absorbed. Over the years, significant efforts have been made in developing visible light-absorbing TiO_2-based photocatalysts.[1] Promising strategies can be the development of localized surface plasmon resonance photosensitization or electromagnetic field enhancement using noble metal nanoparticles.[2-7] Electrons excited in the noble metal can be transferred through the interface to the conduction band of TiO_2 in a composite nanomaterial, and therefore, visible light can be utilized. Alternatively, the excitation efficiency of TiO_2 is enhanced by the electromagnetic field of metal particles. In both scenarios, a closed interface between the metal and TiO_2 is greatly favorable.

Core–shell composite architecture can be a perfect option for offering such interface.[8, 9] The noble metal core possesses plasmonic properties that can be well tailored by designing the composition and shape, while the composition, thickness, and structure of the semiconductor shell can also be finely tuned. Moreover, strong interactions between the core and shell endow the core–shell structure with new properties,[10] and the

photocatalytic properties of TiO_2 can be greatly enhanced.[6] Since the pioneer work of silica coating by Liz-Marzan et al.,[11] approaches towards the synthesis of metal–oxide core–shell composite nanostructures have attracted a great deal of attention in recent years.[12] Pastoriza-Santos et al. introduced one-pot method for the synthesis of Ag@TiO_2 core–shell nanoparticles.[13] Mayya et al. successfully coated TiO_2 on gold nanoparticles in aqueous solutions through a sol–gel method.[14] The sol–gel approach was further improved and modified by many groups by varying the capping agents, TiO_2 precursor, solution mixture, and temperature to achieve desired core shell structures.[15-18] However, these approaches generally involve multistep processes which require additional steps for the ligand exchange or encapsulation of an intermediate coating layer.

Mesoporous structure is of particular significance in photocatalysis because enhanced charge separation,[4] high surface area, and high surface-to-volume ratio brought by the porous structure is beneficial to the photocatalytic performance.[8] Hydrothermal method was employed to achieve porous structure of the TiO_2 shell.[19] The shell is usually very rough, which is related with the disordered mesophases of TiO_2. Mesoporous TiO_2 shell was also obtained by using a sol–gel method.[20, 21] However, these modified Stöber methods are not directly applicable to cetyl-trimethylammonium bromide (CTAB)-capped nanoparticles because those are not stable in alcoholic solutions. Ligand exchange or surface encapsulation in such cases is necessary. Soft template method has been widely used to synthesize mesoporous TiO_2 (mTiO_2) nanomaterials, where the formation of TiO_2 networks usually involve the using of structure-directing agents, including block copolymers[22] and charged surfactant molecules, such as CTAB.[23] It is advantageous because the mesostructures can be easily controlled by the template molecules. Gorelikov et al. introduced the template method for the mesoporous silica coating of gold nanorods (AuNRs).[24] Previous attempts succeed in direct coating TiO_2 on CTAB-capped metal nanoparticles. However, usually a thin TiO_2 layer without

a. Division of i-Lab & Key Laboratory for Nano-Bio Interface Research, Suzhou Institute of Nano-Tech & Nano-Bionics, Chinese Academy of Sciences, Suzhou, Jiangsu, 215123, China
b. Materials Science and Engineering School, Luoyang Institute of Science and Technology, Luoyang, Henan, 471023, China
* Corresponding author: whni2012@sinano.ac.cn
Electronic Supplementary Information (ESI) available: Experimental details including chemicals, sample preparation, and characterization methods. UV–Vis extinction spectra, SEM images, and TEM images of AuNR@mTiO2 nanostructures are included. See DOI: 10.1039/x0xx00000x

mesoporous structure was obtained.[25, 26] Direct coating of $mTiO_2$ on metal nanoparticles is rarely reported in literature.
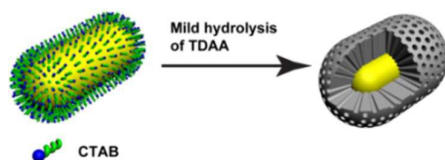
Scheme 1. Schematic illustration of the template-mediated $mTiO_2$ coating on the CTAB-capped AuNR.

Herein, we demonstrate a CTAB-templated approach towards direct coating of $mTiO_2$ on AuNRs in aqueous solutions through finely controlling the reaction rate. CTAB concentration is proved very critical to the formation of mesoporous structure. The $mTiO_2$ shell thickness can be readily tuned. The approach is very reproducible and does not involve any intermediate coating procedures, which drastically improves the interfacial contact as well as the overall yield. The approach can be readily extended to form $mTiO_2$ shells on other CTAB-capped nanoparticles. The $mTiO_2$ shell is uniform, smooth, and characteristic of mesoporous structure, while the AuNR core possesses a longitudinal surface plasmon resonance (LSPR) that can be finely tuned from visible to near infrared range. Furthermore, efficient generation of $^1O_2$ is observed on the AuNR@$mTiO_2$ nanostructures under resonant plasmon excitation. These highly uniform nanostructures with tunable LSPR photosensitization wavelength can be of great potential in a variety of energy and environment applications.
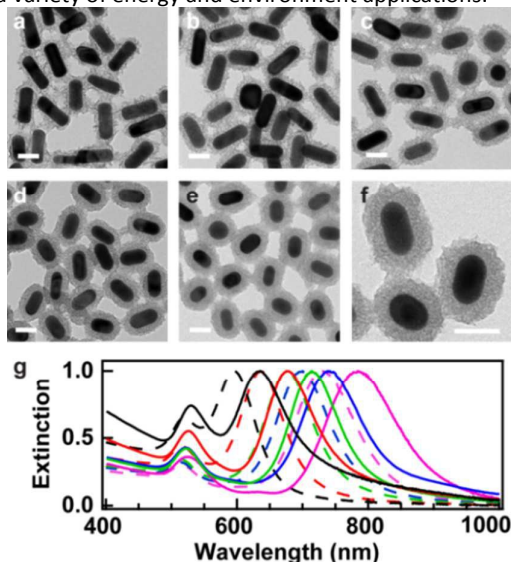

Fig. 1. AuNR@$mTiO_2$ nanostructures with various AuNR aspect ratios. (a–e) TEM images of AuNR@$mTiO_2$ nanostructures with decreasing AuNR aspect ratios. (f) Magnified TEM image of (e) clearly showing the mesoporous structure of the $mTiO_2$ shell. The scale bars are 50 nm. (g) Corresponding normalized extinction spectra of AuNR samples before (dashed lines) and after (solid lines) the $mTiO_2$ coating.

AuNRs were synthesized using the seed-mediated method.[27] Their sizes are relatively uniform as shown in the transmission electron microscopy (TEM) image (Fig. S1a). Five

AuNR samples with ensemble LSPR wavelengths 730, 698, 675, 637, and 597 nm (Fig. S1) were prepared by using the hydrogen peroxide-method introduced in our previous work.[28, 29] Scheme 1 illustrates the CTAB-templated approach towards direct coating of $mTiO_2$ on AuNRs. Briefly, the CTAB concentration of the reaction solution was finely controlled and optimized at around 0.18 mM, and the pH was tuned to around 10.5. The coating was performed using titanium diisopropoxide bis(acetylacetonate) (TDAA), a TiO_2 precursor with slow hydrolysis rate. To maintain a very mild hydrolysis, 100 μL of TDAA methanol solution (V_{TDAA}: V_{MeOH} = 1: 100) was carefully added (every 0.5–1 hr, 10–15 μL at a time) to 6.7 mL of the reaction solution under vigorous stirring. The mild hydrolysis and condensation of TDAA resulted in uniform core–shell AuNR@$mTiO_2$ nanostructures (Fig. 1a–e). Our method is very reproducible, and the product is well monodispersed as shown in the scanning electron microscopy (SEM) images (Fig. S2).

Although TDAA amount was kept the same for the five samples, the thickness of the $mTiO_2$ shells increases from 11 to 28 nm with the decrease of AuNR aspect ratio, which is due to the decreasing surface area of the AuNRs. The mesoporous structure of the shell can be clearly observed in a magnified TEM image (Fig. 1f). It is surprisingly similar to that of the mesoporous silica shell shown in the previous report,[24] where one can hardly distinguish them solely from the TEM images. This similarity suggests the same role of CTAB molecules as the soft template in the formation of the mesoporous structures. As shown in the UV–vis spectra (Fig. 1g), the LSPR shifts toward a longer wavelength as the shell is grown due to the refractive index change around the AuNRs. The index change-induced plasmon shift increases from 37 to 54 nm with the increase of the aspect ratio (Table S1), which can be attributed to the increasing index sensitivity of AuNRs.[30]
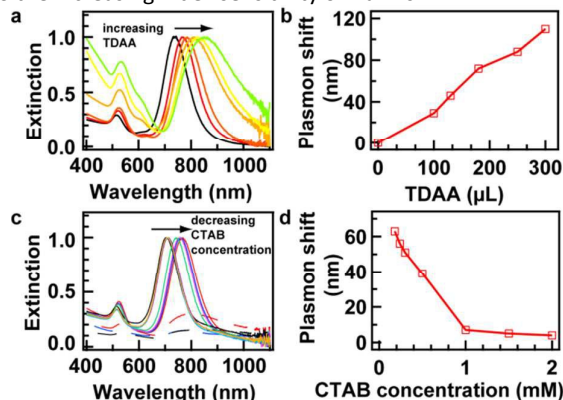

Fig. 2. Effects of TDAA and CTAB on the formation of $mTiO_2$ shell. (a) Normalized extinction spectra of AuNR@$mTiO_2$ samples prepared with various TDAA amount. (b) Plasmon shift as a function of TDAA amount. (c) Those prepared with various CTAB concentration. CTAB below 0.122 mM (dashed lines) and from 0.18 to 2 mM (solid lines) are shown. (d) Plasmon shift as a function of CTAB concentration.

The thickness of the $mTiO_2$ shell can be readily tuned by varying the amount of TDAA added to the reaction solution.

The LSPR peak gradually performs red shift with the increase of the TDAA amount, where a largest plasmon shift 110 nm is observed (Fig. 2a and b). A linear correlation is found between the plasmon shift and TDAA amount (Fig. 2b). The shell thickness increases from 11 to 30 nm when the amount of TDAA is increased from 100 to 300 μL (Fig. S3), suggesting complete hydrolysis of TDAA on AuNR surface. More importantly, CTAB concentration in the reaction solution is found very critical for the formation of the shell. The plasmon shift generally increases with decreasing CTAB concentration (Fig. 2c, d, and Fig. S4). With the decrease of concentration lower than 1 mM, the critical micelle concentration (cmc)[31] of CTAB molecules, it increases drastically and reaches a maximum of 63 nm at the corresponding CTAB concentration 0.18 mM. Further decrease of the concentration leads to the aggregation of AuNRs during the reaction (dashed lines, Fig. 2c and Fig. S4a–c). Thin shells can be found at relatively high CTAB concentrations (Fig. S4g and h). A control experiment without the Au core was performed, indicating the decrease of TDAA hydrolysis rate with increasing CTAB concentration. It suggests that CTAB stabilizes TDAA and protects it from hydrolysis due to the affinity between CTAB and TDAA molecules. The thickness of the TiO_2 shell is less than 5 nm in the previous reports,[25, 26] which can be related with the presence of CTAB with relatively high concentration (larger than cmc) in their reaction solutions.
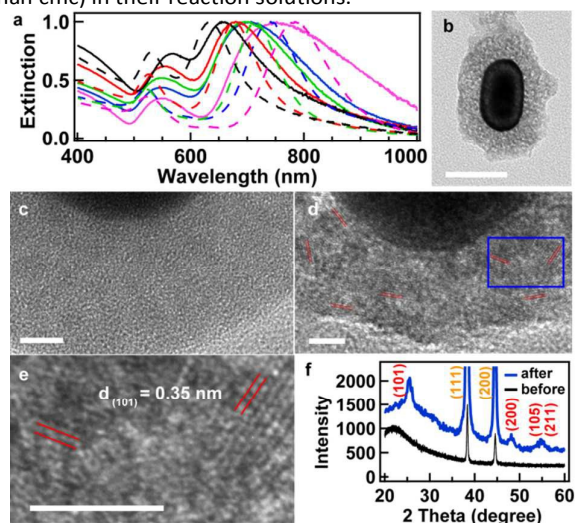

Fig. 3. Calcination of AuNR@$mTiO_2$ nanostructures. (a) Normalized extinction spectra before (dashed lines) and after (solid lines) calcination. (b) TEM image of a typical AuNR@$mTiO_2$ nanostructure after the calcination. Scale bar 100 nm. (c) and (d) HRTEM images before and after the calcination, respectively. (e) Zoomed-in image for the area highlighted in (d). The lattice spacing is 0.35 nm (red lines). Scale bars 5 nm. (f) XRD patterns before and after the calcination with Au (orange numbers) and anatase phase of TiO_2 (red numbers) diffraction peaks indexed.

To investigate the crystallinity of the $mTiO_2$ shells, the synthesized AuNR@$mTiO_2$ nanostructures were subjected to calcination in air ambiance at 450 °C for 2 hr. Extinction

spectra were obtained from the AuNR@$mTiO_2$ nanostructure films after the calcination. Interestingly, the thermal treatment has different effects on the core–shell structures with various aspect ratios. The longitudinal plasmon peaks of the sample with small (large) AuNR aspect ratios shift to longer (shorter) wavelengths (Fig. 3a and Table S2). To understand the result, the calcinated nanostructures were sonicated from the substrates to the solutions and deposited on TEM grids. The calcination results in both decrease of the length and slight increase of the width (Table S2) and hence shrinking of the aspect ratio to different extent (Fig. S5), depending on the initial aspect ratio of AuNRs. The shrink of the shell is found together with the core (Fig. 3b), suggesting the elastic nature of the $mTiO_2$ shell, which is consistent with the observation on mesoporous silica in the previous report.[32] Meanwhile, the crystallinity of the $mTiO_2$ shell is significantly improved as revealed by the high-resolution TEM (HRTEM) and X-ray diffraction (XRD) measurements. After the calcination, the amorphous $mTiO_2$ (Fig. 3c) starts to form polycrystalline particles (Fig. 3d and e). The observed lattice spacing is 0.35 nm, which matches well to the d_{101} of anatase TiO_2.[33] The anatase phases are observable in the XRD pattern after calcination (Fig. 3f). Therefore, the observed plasmon shift can be ascribed to the sum effect of the index increase around the AuNRs due to improved crystallinity of the $mTiO_2$ shell and the shrink of the aspect ratio whose extent is related with the initial aspect ratio.
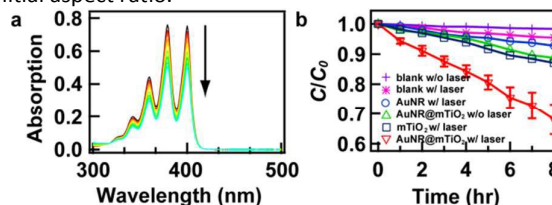

Fig. 4. Generation of $^1O_2$ using AuNR@$mTiO_2$ nanostructures. (a) Time evolution of ABDA absorption spectra under irradiation in the presence of AuNR@$mTiO_2$. (b) Time-dependent normalized absorbance of ABDA under irradiation. The error bars are a standard deviation from the mean.

AuNR@$mTiO_2$ solution sample with LSPR at 784 nm (Fig. 1a) was employed in the photodynamic therapy experiments. A diode laser at 808 nm and 210 mW was chosen as the excitation source. $^1O_2$ can be generated by a series of reactions involving photon-generated electrons and holes in Au and TiO_2.[17] 9,10-anthracenediyl-bis(methylene) dimalonic acid (ABDA) with UV absorption bands was employed as the probe molecule for monitoring the generation of $^1O_2$.[17] Its absorption is decreased when ABDA reacts with $^1O_2$ to produce endoperoxide. During the measurement, the solution mixture was irradiated in a quartz cuvette at 656 mW cm^{-2} under vigorous stirring. The temperature of the solution increased by 2-3 °C from room temperature after 30 min irradiation, suggesting a negligible thermal effect. The absorption spectra of the ABDA solution were recorded every 1 hr after removing the nanostructures by centrifugation (Fig. 4a and Fig. S6). Compared to the blank sample, the AuNR sample (Fig. S7) shows slightly higher rate at resonant plasmon

excitation (Fig. 4b), which can be ascribed to the scattering of incident light by the AuNRs in the solution. The AuNR@mTiO$_2$ samples exhibit a rate that is 2.5 folds higher than that of the hollow TiO$_2$ structures (Fig. 4b). This result is consistent with that previously reported.[17] The apparent quantum efficiency[4, 34] for the AuNR@mTiO$_2$ sample is evaluated to be 0.072%.

Mechanisms have been proposed for the visible-light photosensitization of Au/TiO$_2$ structures, which are related with the excitation of LSPR. Hot electrons excited in Au can transfer through the interface to the conduction band of TiO$_2$.[2, 4] On the other hand, surface defects on TiO$_2$ can be electromagnetically coupled with the LSPR of Au nanoparticles.[3, 16] In both processes, several factors are considered crucial. i) excitation efficiency of the LSPR. The difference between the excitation and LSPR wavelengths determines the final photocatalytic activity. As we have demonstrated, the LSPR of the synthesized nanostructures can be freely tuned from the visible to NIR range, which enables perfect match of the two. ii) contact interface between the semiconductor and the metal. Direct contact between Au and TiO$_2$ is a prerequisite for efficient transfer of the electrons, which can be realized by the direct coating of TiO$_2$ on AuNRs. CTAB as a nonconducting material can be removed either by washing in alcoholic solutions or by calcination at high temperatures. iii) mesoporous structure. The mesoporous structure facilitates the charge separation[4] and efficient exchange of molecules, and also provides the possibility for the core to be involved in the catalytic reactions.[2]

In conclusion, we have demonstrated a CTAB-templated approach towards direct coating of mTiO$_2$ on AuNRs through finely controlling the reaction conditions. Effects of TDAA and CTAB on the shell thickness are studied in detail. The crystallinity of the shells is characterized before and after the calcination at elevated temperatures. Efficient generation of ^{1}O$_2$ is observed on the AuNR@mTiO$_2$ nanostructures under resonant plasmon excitation.

Acknowledgement

References

1.   X. Chen and S. S. Mao, *Chem. Rev.* , 2007, **107**, 2891.
2.   C. G. Silva, R. Juarez, T. Marino, R. Molinari and H. Garcia, *J. Am. Chem. Soc.* , 2011, **133**, 595.
3.   T. Tachikawa, T. Yonezawa and T. Majima, *Acs Nano*, 2013, **7**, 263.
4.   Z. F. Bian, T. Tachikawa, P. Zhang, M. Fujitsuka and T. Majima, *J. Am. Chem. Soc.* , 2014, **136**, 458.
5.   M. W. Knight, H. Sobhani, P. Nordlander and N. J. Halas, *Science*, 2011, **332**, 702.
6.   K. Awazu, M. Fujimaki, C. Rockstuhl, J. Tominaga, H. Murakami, Y. Ohki, N. Yoshida and T. Watanabe, *J. Am. Chem. Soc.* , 2008, **130**, 1676.
7.   Q. Zhang, D. Q. Lima, I. Lee, F. Zaera, M. F. Chi and Y. D. Yin, *Angewandte Chemie-International Edition*, 2011, **50**, 7088.
8.   Y. P. Xie, Z. B. Yu, G. Liu, X. L. Ma and H. M. Cheng, *Energy Environ. Sci.* , 2014, **7**, 1895.
9.   Y. Q. Yang, C. H. Sun, L. Z. Wang, Z. B. Liu, G. Liu, X. L. Ma and H. M. Cheng, *Advanced Energy Materials*, 2014, **4**, 1400057.
10.   T. Hirakawa and P. V. Kamat, *Langmuir*, 2004, **20**, 5645.
11.   L. M. Liz-Marzan, M. Giersig and P. Mulvaney, *Langmuir*, 1996, **12**, 4329.
12.   A. Guerrero-Martinez, J. Perez-Juste and L. M. Liz-Marzan, *Adv. Mater.* , 2010, **22**, 1182.
13.   I. Pastoriza-Santos, D. S. Koktysh, A. A. Mamedov, M. Giersig, N. A. Kotov and L. M. Liz-Marzan, *Langmuir*, 2000, **16**, 2731.
14.   K. S. Mayya, D. I. Gittins and F. Caruso, *Chem. Mater.* , 2001, **13**, 3833.
15.   Z. W. Seh, S. Liu, S.-Y. Zhang, M. S. Bharathi, H. Ramanarayan, M. Low, K. W. Shah, Y.-W. Zhang and M.-Y. Han, *Angewandte Chemie-International Edition*, 2011, **50**, 10140.
16.   X. Zhang, Y. Zhu, X. Yang, S. Wang, J. Shen, B. Lin and C. Li, *Nanoscale*, 2013, **5**, 3359.
17.   C. H. Fang, H. L. Jia, S. Chang, Q. F. Ruan, P. Wang, T. Chen and J. F. Wang, *Energy Environ. Sci.* , 2014, **7**, 3431.
18.   A. Li, P. Zhang, X. Chang, W. Cai, T. Wang and J. Gong, *Small*, 2015, **11**, 1892.
19.   J. Li and H. C. Zeng, *Angew. Chem. Int. Ed. Engl.*, 2005, **44**, 4342.
20.   W. Li, J. Yang, Z. Wu, J. Wang, B. Li, S. Feng, Y. Deng, F. Zhang and D. Zhao, *J. Am. Chem. Soc.* , 2012, **134**, 11864.
21.   W. Zhang, Y. Wang, X. Sun, W. Wang and L. Chen, *Nanoscale*, 2014, **6**, 14514.
22.   P. D. Yang, D. Y. Zhao, D. I. Margolese, B. F. Chmelka and G. D. Stucky, *Nature*, 1998, **396**, 152.
23.   E. Beyers, P. Cool and E. F. Vansant, *J. Phys. Chem. B* 2005, **109**, 10081.
24.   I. Gorelikov and N. Matsuura, *Nano Lett.* , 2008, **8**, 369.
25.   H. Sakai, T. Kanda, H. Shibata, T. Ohkubo and M. Abe, *J. Am. Chem. Soc.* , 2006, **128**, 4944.
26.   N. Zhou, L. Polavarapu, N. Gao, Y. Pan, P. Yuan, Q. Wang and Q.-H. Xu, *Nanoscale*, 2013, **5**, 4236.
27.   T. K. Sau and C. J. Murphy, *Langmuir*, 2004, **20**, 6414.
28.   W. H. Ni, X. S. Kou, Z. Yang and J. F. Wang, *Acs Nano*, 2008, **2**, 677.
29.   Q. N. Zhu, J. Wu, J. W. Zhao and W. H. Ni, *Langmuir*, 2015, **31**, 4072.
30.   W. H. Ni, H. J. Chen, X. S. Kou, M. H. Yeung and J. F. Wang, *J. Phys. Chem. C* 2008, **112**, 8105.
31.   X. R. Huang, J. H. Yang, W. J. Zhang, Z. Y. Zhang and Z. S. An, *J. Chem. Educ.* , 1999, **76**, 93.
32.   E. Gergely-Fueloep, D. Zambo and A. Deak, *Mater. Chem. Phys.* , 2014, **148**, 909.
33.   X. Y. Ma, Z. G. Chen, S. B. Hartono, H. B. Jiang, J. Zou, S. Z. Qiao and H. G. Yang, *Chem. Commun.* , 2010, **46**, 6608.
34.   J. M. Buriak, P. V. Kamat and K. S. Schanze, *ACS Appl. Mat. Interfaces* 2014, **6**, 11815.

TOC